Sonic boom reflection over urban areas

Didier Dragna, Ariane Emmanuelli, S. Ollivier, Philippe Blanc-Benon

JASA ARTICLE

Sonic boom reflection over urban areas

Didier Dragna,[a] Ariane Emmanuelli, Sébastien Ollivier, and Philippe Blanc-Benon
Laboratoire de Mécanique des Fluides et d'Acoustique, Université de Lyon, Ecole Centrale de Lyon, INSA Lyon, Université Claude Bernard Lyon I, CNRS, UMR 5509, 36 Avenue Guy de Collongue, F-69134, Ecully, France

ABSTRACT:
Sonic boom propagation over urban areas is studied using numerical simulations based on the Euler equations. Two boom waves are examined: a classical N-wave and a low-boom wave. Ten urban geometries, generated from the local climate zone classification [Stewart and Oke (2012), Bull. Am. Meteorol. Soc. **93**(12), 1879–1900], are considered representative of urban forms. They are sorted into two classes, according to the aspect ratio of urban canyons. For compact geometries with a large aspect ratio, the noise levels and the peak pressure, especially for the N-wave, are highly variable between canyons. For open geometries with a small aspect ratio, these parameters present the same evolution in each urban canyon, corresponding to that obtained for isolated buildings. A statistical analysis of the noise levels in urban canyons is then performed. For both boom waves, the median of the perceived noise levels mostly differs by less than 1 dB from the value obtained for flat ground. The range of variation is greater for open geometries than for compact ones. Finally, low-frequency oscillations, associated with resonant modes of the canyons, are present for both compact and open geometries. Their amplitude, frequency and decay rate vary greatly from one canyon to another.
 https://doi.org/10.1121/10.0016442
(Received 15 June 2022; revised 19 November 2022; accepted 20 November 2022; published online 7 December 2022)
[Editor: Vladimir E Ostashev] Pages: 3323–3339

I. INTRODUCTION

Noise annoyance due to sonic boom remains one environmental key consideration for supersonic transport. Reduction of sonic boom is thus a long quest and it is a necessary condition for the lifting of the ban on overland civil supersonic flight. Its feasibility has been shown by reshaping supersonic military aircraft (Pawlowski *et al.*, 2005). The X-59 experimental aircraft (NASA, 2021) has been specifically designed to generate a so-called low boom in order to evaluate the public's response to this reduced boom in the coming years.

If the overland ban is lifted, commercial routes will likely pass over densely populated areas. In addition to boom reduction, prediction of the boom at the ground and of the corresponding annoyance is thus of major concern in urban environments. In particular, it is necessary to evaluate how the urban environment impacts the boom signature compared to the ideal case of flat ground.

Studies in the literature have been mostly concerned with the diffraction of a sonic boom by an isolated building (Maglieri *et al.*, 2014). They have been performed using experiments (Bauer and Bagley, 1970; Brooks *et al.*, 1970), analytical formulations (Ting and Pan, 1968) or, more recently, numerical simulations (Cho and Sparrow, 2011; Dragna *et al.*, 2022; Yamashita and Nikiforakis, 2021). Two significant zones around the building were highlighted: an illuminated zone at its front and a shadow zone at its back. The perceived noise levels were shown to increase by at most 7–9 dB in the illuminated region compared to the flat ground case, whether the boom was an N-wave or a low-boom wave, and to decrease largely in the shadow zone depending on the building height.

Recently, Dragna *et al.* (2022) investigated sonic boom reflection over multiple buildings for academic geometries. To this end, numerical simulations based on the Euler equations were performed. Two main effects were highlighted in the street canyons. The first one is related to reflection of sonic boom on the facades of the buildings and on the street, which generates additional geometric contributions to the pressure field, compared to flat ground. This effect was shown to be governed by the aspect ratio of the street canyon, defined as the ratio of the building height to the street width. The second effect was the presence of low-frequency oscillations at the tails of the waveforms related to local modes of the urban canyon. The amplitude of these oscillations depends on both the urban geometry and the incident sonic boom. The influence of these two phenomena on the perceived noise levels was investigated. For widely spaced buildings, corresponding to a small aspect ratio, the noise levels were similar to those for isolated buildings. As the aspect ratio increases, the levels were noted to be amplified in the shadow zone behind the building and reduced in the illuminated region at its front. This tends to make the noise levels uniform over the urban canyon. Finally, the canyon resonances have little impact on the levels.

[a]Electronic mail: didier.dragna@ec-lyon.fr

This paper pursues the study of sonic boom propagation over urban environments by considering realistic urban geometries. With this aim, a recent classification of urban configurations proposed in the literature is employed to generate ten profiles, representative of urban environments. The acoustic pressure field is analyzed and compared. The statistics of the perceived noise levels for the ten profiles are then examined.

The paper is organized as follows. The geometry of the ten profiles and the propagation model is described in Sec. II. Section III shows the variability of the boom signature depending on the geometric properties of the urban forms. A detailed analysis of the boom characteristics is performed in Sec. IV for two urban profiles. A statistical analysis of the perceived noise levels for the ten profiles is conducted in Sec. V. Finally, concluding remarks are given in Sec. VI.

II. CONFIGURATIONS AND METHODOLOGY

Sonic boom propagation above realistic urban sections is investigated, as sketched in Fig. 1, using numerical simulations. In order to have an acceptable computational cost, two-dimensional (2D) configurations are considered. The buildings thus have an infinite length in the direction perpendicular to the plane of 2D calculation. This neglects the inherent diffraction at the side edges for buildings of finite length. As shown in Fig. 1, the aircraft is flying from left to right and the generated boom propagates rightwards.

A. Configurations

The geometries of urban areas originate from the "local climate zone" (LCZ) classification proposed by Stewart and Oke (2012). While it has been initially developed for studies on urban heat islands, the LCZ classification allows for a convenient approach to differentiate the urban configurations. Seventeen LCZ classes are defined, with ten built types and seven land cover types. Only the ten built types (LCZ 1-10) are considered thereafter. The standard defines for each LCZ, besides the geometry of the buildings, the land cover, and the presence or absence of vegetation. This study only focuses on the urban geometry and a bare and perfectly reflecting ground is considered.

More in detail, LCZ 1-3 correspond to compact arrangements of buildings, which are typical of densely populated areas. They differ in the height of the buildings: LCZ 1 consists of high-rise buildings, LCZ 2 of midrise buildings and LCZ 3 of low-rise buildings. LCZ 4-6 are similar to LCZ 1-3 with respect to building height but present a larger space between the buildings. LCZ 7 represents small closely packed buildings, that can be encountered in shanty towns. LCZ 8 is made of large low-rise buildings, corresponding for instance to shopping centres or warehouses. LCZ 9 consists of small or medium-sized buildings widely spaced, as in rural towns or the periphery of urban centres. Finally, LCZ 10 represents heavy industry structures.

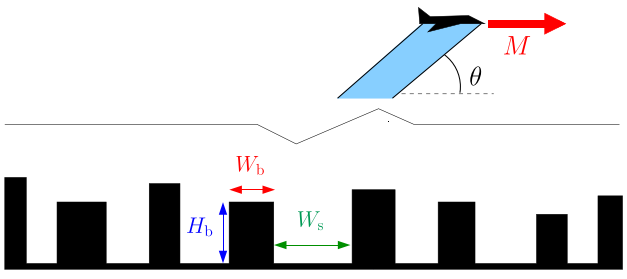

FIG. 1. (Color online) Sonic boom propagation over an urban area.

Some examples on the proportion of built area occupied by each LCZ class are given in Table I for selected cities. Data for Paris, France, are for Greater Paris, that corresponds to Paris and its nearest surrounding suburbs. The city of Paris alone is composed predominantly of LCZ 2 (almost 80% of the city area) and LCZ 5 (near 10%) (Hidalgo *et al.*, 2019). Data for Milan, Italy, is for a part of the Milan metropolitan area and includes the city of Milan and smaller satellite cities. As a consequence, the proportion of built area with low population density, corresponding to LCZ 9, is large. Data for Shangai, China, covers only downtown Shangai. Finally, data for Chicago, Sao Paolo, and Vancouver are for the entire cities. The variety of LCZ composition for the different cities can be especially noticed. Note also that LCZ maps are currently developed at the global scale (Demuzere *et al.*, 2022).

For each LCZ class, the geometry of the urban section is generated using the properties given in Table II, derived from the LCZ standard and assuming rectangular buildings. The corresponding urban sections of 900 m long are shown for the ten LCZ classes in Fig. 2. A profile length of 900 m was chosen in order to have a sufficient number of buildings to be representative of LCZ classes while maintaining an affordable computational cost. The height and the width of buildings, denoted by H_b and W_b, respectively, and the street width W_s are generated randomly using a uniform distribution. The min and max values are chosen to target the reference values indicated in the LCZ standard of the aspect ratio (AR), the building surface fraction (BSF), and the height of buildings. The (global) aspect ratio is defined as the mean height-to-width ratio of street canyons, i.e.,

$$\mathrm{AR} = \bar{H}_b/\bar{W}_s, \tag{1}$$

where the overline denotes the mean value. The building surface fraction corresponds to the ratio of building plan area to total plan area, which is approximately $\mathrm{BSF} \approx \bar{W}_b/(\bar{W}_s + \bar{W}_b)$.

Because this study focuses on reflection over urban areas, the atmosphere is considered homogeneous and at rest for simplicity. The sound speed is set to $c_0 = 340\ \mathrm{m\ s^{-1}}$ and the air density to $1.22\ \mathrm{kg\ m^{-3}}$. In addition, the roofs and facades of the buildings are perfectly reflecting.

The flight Mach number is set to $M = 1.6$. The angle of the incident boom wavefront from the horizontal θ (see Fig. 1) is then given by $\sin\theta = 1/M$ for a homogeneous atmosphere at rest. It is thus equal to $\theta = 38.7°$ for all simulations reported in this work.

https://doi.org/10.1121/10.0016442

TABLE I. Proportion of built area occupied by each LCZ class (%) for several cities. Adapted from Hidalgo *et al.* (2019) and Ching *et al.* (2018).

	Paris, France	Chicago, USA	Milan, Italy	Sao Paolo, Brazil	Shangai, China	Vancouver, Canada
LCZ 1	1.2	2.3	0.0	3.8	4.9	1.7
LCZ 2	31.3	2.6	8.7	0.4	23.6	0.1
LCZ 3	13.5	4.3	0.4	35.0	6.8	5.0
LCZ 4	9.7	9.1	7.5	1.6	17.0	6.3
LCZ 5	14.0	2.6	22.2	2.3	17.4	0.0
LCZ 6	19.5	58.4	0.5	21.0	3.5	76.4
LCZ 7	0.0	0.0	0.0	4.6	2.3	0.0
LCZ 8	10.6	14.2	14.7	13.2	5.7	6.1
LCZ 9	0.2	3.0	46.0	16.9	0.1	4.4
LCZ 10	0.0	3.5	0.0	1.2	18.7	0.0

Simulations are performed for two incident boom waves, an N-wave and a low-boom wave, which have been already considered by Emmanuelli *et al.* (2021) and Dragna *et al.* (2022). For completeness, the time signals of the incident booms and the corresponding (one-sided) energy spectral densities (ESD) are shown in Fig. 3. The ESD is computed with $\mathrm{ESD}(f) = 2|\hat{p}(f)|^2$, where $\hat{p}(f)$ is the Fourier transform of the time signal of the acoustic pressure $p'(t)$. The N-wave has a peak value p_{ind} equal to 24 Pa, a rise time of 0.0011 s, and a duration $T = 0.15$ s, corresponding to a characteristic wavelength $c_0 T = 51$ m. (For information, the width of the boom footprint is equal to Mc_0T, yielding about 82 m for the N-wave.) The signal energy of the N-wave is significant up to a few kHz. The low-boom wave, referred to as the C25D wave, originates from a notional configuration, used in the 2nd AIAA Sonic Boom Workshop (Rallabhandi and Loubeau, 2019). The boom wave was obtained by propagating the near-field signature down to the ground using the BANGV nonlinear ray tracing code (Loubeau and Coulouvrat, 2009). The C25D wave has a peak value of 20 Pa, a rise time of 0.014 s, and a duration of about 0.1 s, corresponding to a characteristic wavelength of 34 m. Due to the large rise time, most of the frequency content of the boom wave is below 800 Hz. Note that on a perfectly reflecting ground without buildings, the peak pressure is expected to be 48 Pa for the N-wave and 40 Pa for the C25D wave, due to pressure doubling.

A preliminary indication can be made on boom propagation over the ten LCZ. It was shown in Dragna *et al.* (2022) that the key parameter governing the reflection of the boom within an urban canyon was its aspect ratio. More precisely, for $\mathrm{AR} < \mathrm{AR}_1$, with $\mathrm{AR}_1 = \sqrt{M^2 - 1}/2$, reflection over each building of the urban geometry is similar to that over an isolated building: the geometric arrivals around a given building are not influenced by the surrounding ones. For $\mathrm{AR} > \mathrm{AR}_1$, multiple reflections occur on the opposing facades of the neighbouring buildings in the urban canyon. This effect is amplified by the increase in AR. For $M = 1.6$, one has $\mathrm{AR}_1 = 0.63$. From Table II, note that the aspect ratio is larger than AR_1 for LCZ 1, 2, 3, 4, and 7 and smaller than AR_1 for LCZ 5, 6, 8, 9, and 10. The former type of LCZ will be referred to as *compact* and the latter as *open*, thereafter.

B. Equations and numerical methods

The 2D Euler equations are solved using finite-difference time-domain techniques, developed for computational aeraocoustics (Bogey and Bailly, 2004). The solver is described in detail in Emmanuelli *et al.* (2021) and only the main elements are summarized thereafter.

TABLE II. Parameters of the generated urban section for each LCZ class: range of the building height H_b, building width W_b and street width W_s, and numbers of buildings N_b. The target values of aspect ratio AR (mean height-to-width ratio of street canyons) and building surface fraction BSF (ratio of building plan area to total plan area) from the LCZ standard and the deduced values from the generated sections are also provided. Sonic boom propagation over LCZ 2 and 5 is discussed in details in Sec. IV.

LCZ		Design variables				Target values		Deduced values	
	Name	H_b, m	W_b, m	N_b	W_s, m	AR	BSF (%)	AR	BSF (%)
LCZ 1	Compact high-rise	25–50	10–20	30	10–15	> 2	40–60	2.8	54
LCZ 2	Compact midrise	10–20	10–20	30	10–15	0.75–2	40–70	1.3	53
LCZ 3	Compact low-rise	3–10	10–15	40	5–10	0.75–1.5	40–70	0.9	64
LCZ 4	Open high-rise	25–50	10–20	18	20–40	0.75–1.25	20–40	1.1	34
LCZ 5	Open midrise	10–20	10–20	18	20–40	0.3–0.75	20–40	0.5	33
LCZ 6	Open low-rise	3–10	10–15	25	15–25	0.3–0.75	20–40	0.4	39
LCZ 7	Lightweight low-rise	2–4	3–5	130	1.5–2.5	1–2	60–90	1.5	67
LCZ 8	Large low-rise	3–10	20–40	13	25–50	0.1–0.3	30–50	0.2	49
LCZ 9	Sparsely built	3–10	3–10	20	25–45	0.1–0.25	10–20	0.2	16
LCZ 10	Heavy industry	5–15	15–25	14	35–50	0.2–0.5	20–30	0.2	33

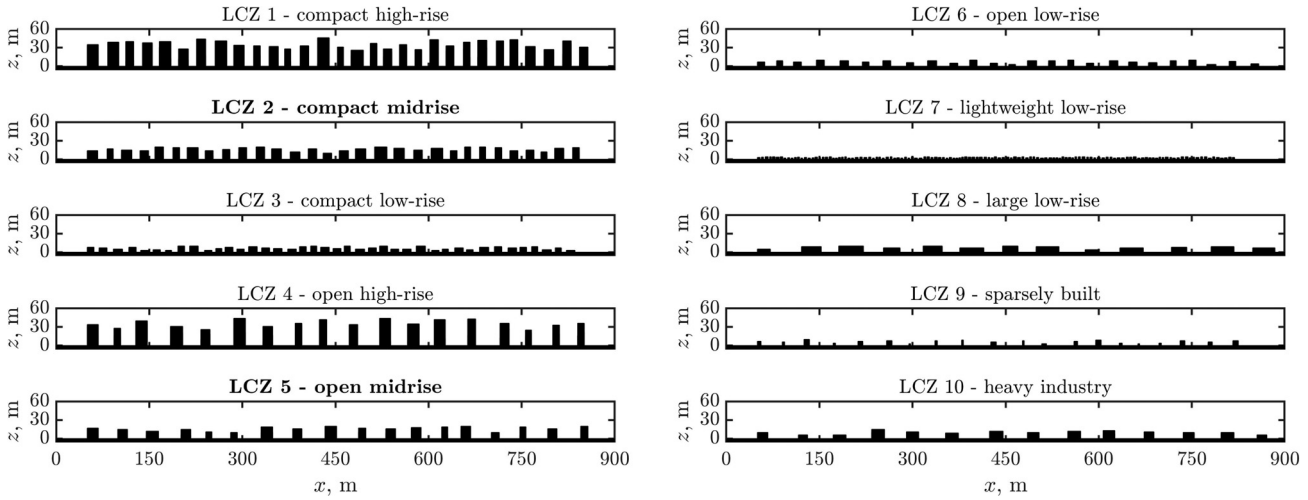

FIG. 2. Urban sections generated for the ten LCZ. The same scale is used for the x and z-axes.

A moving frame, that advances at the same speed as the aircraft, is implemented to reduce the computational cost. The incident boom is injected at the right boundary. Note that the waves reflected on the buildings never reach the right boundary because the speed of the moving frame is supersonic. On the top boundary, a perfectly matched layer is used as a non-reflecting boundary condition. On the ground and on the building walls, the normal velocity is set to zero. On the left boundary of the moving frame, no particular strategy is implemented: as the moving frame advances at supersonic speed, the acoustic waves leave the computational domain without generating spurious waves.

C. Numerical parameters

The size of the moving frame domain is $L \times H$ with $L = 800$ m and $H = 200$ m. The motivations for the choice of the moving frame size are detailed in this paragraph. First, because of the moving frame approach, information at a given point is obtained only when it is located within the moving frame. The useful duration of the time signal $\Delta\tau$ is related to the length of the moving frame L and to its speed via $\Delta\tau = L/(Mc_0)$. A longer moving frame allows for a longer duration of the signal but increases the computational cost; a trade-off has thus to be made. With $L = 800$ m, the useful duration of the signal is 1.47 s, which was deemed sufficient to include the geometrical arrivals and a significant part of the post-boom low-frequency oscillations. Second, the incident boom must be injected at an appropriate height, so that it is not truncated by the buildings as the moving frame is advancing. As the maximum building height is 50 m (for LCZ 1), the bottom of the boom wave is injected at a height of 60 m for all simulations and for both boom waves. A height of the moving frame equal to $H = 200$ m is thus sufficient to inject the incident boom wave above the buildings.

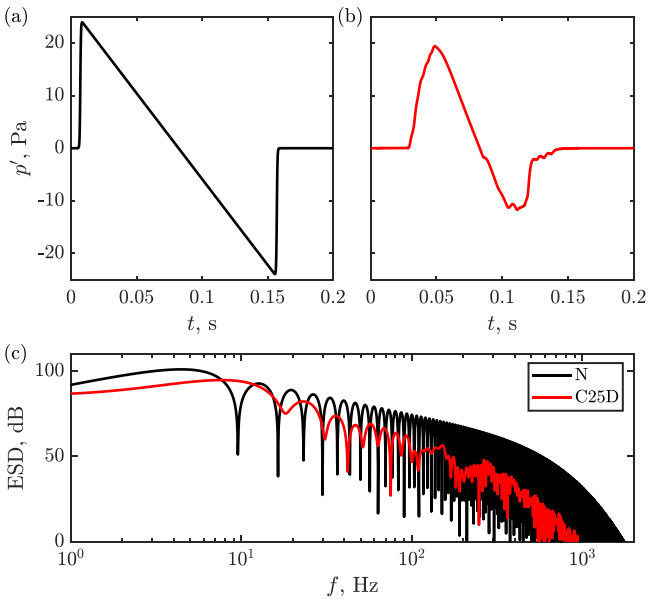

FIG. 3. (Color online) Time signals of the incident boom: (a) N-wave and (b) C25D wave. (c) Corresponding ESDs levels (reference 4×10^{-10} Pa^2/Hz^2).

The mesh is uniform in both directions, i.e., $\Delta x = \Delta z$. The mesh size is chosen according to the convergence study performed in Emmanuelli *et al.* (2021). It is set to $\Delta x = 0.05$ m for the simulations with the N-wave. It is increased to 0.1 m for the C25D wave, except for LCZ 7 for which the mesh size is kept to 0.05 m. The number of points is thus of 16×10^6 points for $\Delta x = 0.1$ m and 64×10^6 points for $\Delta x = 0.05$ m.

The moving frame is shifted along the x-direction by a spatial step every two iterations. The time step is thus set to $\Delta t = \Delta x/(2Mc_0)$ to ensure that the incident sonic boom is stationary in the moving frame. The Courant-Friedrichs-Lewy (CFL) number is then equal to $\mathrm{CFL} = 1/(2M) \approx 0.31$.

The simulation time is set to 1.8 s, which is sufficient for the incident boom to travel over the urban section of 900 m long. The number of iterations is thus 70 000 for the simulations with $\Delta x = 0.05$ m and 35 000 for those with $\Delta x = 0.1$ m.

Simulations are run using 32 core nodes of Intel 6142 Skylake with a clock frequency of 2.6 GHz. The total CPU

https://doi.org/10.1121/10.0016442

time is about 8000 h for the simulations with $\Delta x = 0.05$ m and 1000 h for those with $\Delta x = 0.1$ m.

III. COMPARISON OF THE ACOUSTIC PRESSURE FIELD

An overview of the acoustic pressure field is given for the ten LCZ, both above the urban canopy and inside the street canyons.

A. Above the urban canopy

A snapshot of the acoustic pressure is shown in Fig. 4 for the ten LCZ and for the N-wave. To improve the visualization of the shocks, schlieren-like pictures are overlaid on the maps of pressure. They have been obtained by calculating the gradient of the pressure $\nabla p'$. The contour lines of $|\nabla p'|$ have then been computed and those above a given threshold, selected to highlight shocks, are plotted in black. For ease of interpretation, a sketch depicting the reflection pattern is plotted in Fig. 5. As a reminder, the incident boom, injected at the right boundary of the moving frame, propagates rightwards. Above the urban canopy, the acoustic field is composed of different contributions. The specularly reflected boom is split into two parts. The first one is related to the reflection on the roofs of the buildings and the second to the reflection on the streets. The former has a small amplitude for most of the urban geometries. This is due to the small width of the buildings compared to the boom length, that limits the specular reflection on the roof. Note however that the amplitude of the reflected boom on the roofs is similar to that of the reflected boom on the street for LCZ 8, that is made of large buildings. Also, diffracted waves propagating leftwards are noted; they have been generated by the interaction of the incident boom with the buildings. Their pattern and amplitude strongly depend on the urban form. Thus, the diffracted waves are of noticeable amplitude for open urban geometries with midrise buildings (LCZ 5, 8, and 10) and also for LCZ 4 with high-rise buildings. As the building size reduces, their amplitude reduces as well; for instance, compare LCZ 5 and 6. For compact geometries (LCZ 1, 2, 3, and 7), the diffracted waves have a small amplitude and their pattern appears diffuse, which may be related to multiple reflections inside the street canyons.

B. Inside the street canyons

The waveforms inside the street canyons show a large variability for the ten LCZ. The variability is exemplified for LCZ 2 and 5 in Sec. IV.

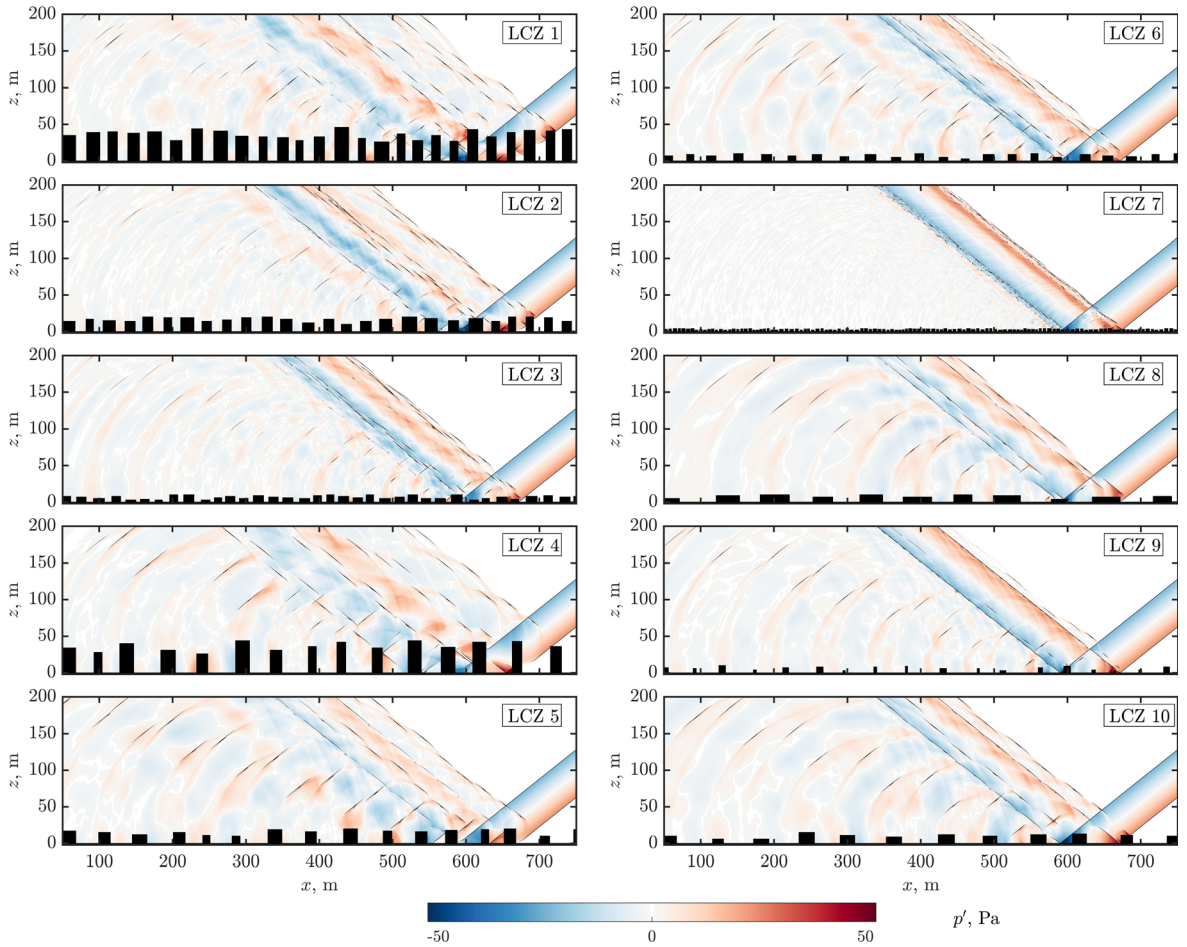

FIG. 4. (Color online) Propagation of the N-wave over the ten urban areas: contour map of the acoustic pressure at the same instant in time. Schlieren-like pictures are overlaid to improve shock visualization. See text for details.

The waveforms having the largest amplitude in the street canyons are selected as a first characterization of the ten LCZ. They were all obtained in buildings' corners, as diffraction by a corner induces a large amplification of the sound pressure. Indeed, a geometrical analysis indicates that an amplification by a factor of four is obtained at a 2D 90° angle corner. As an aside, the amplification factor depends on the solid angle at the corner, as discussed by Ting and Pan (1968). For instance, an amplification by a factor of eight is expected at the three-dimensional 90° angle corner of a L-shaped building.

The waveforms are plotted in Fig. 6 as a function of the reduced time $\tau = t - t_0$, where t is the time and t_0 is the instant at which the acoustic pressure is first larger than 1 Pa. The waveforms for the ten LCZ are composed of a first part for $\tau < 0.2$ s for the N-wave and $\tau < 0.15$ s for the C25D wave with geometric arrivals and a second part with low-frequency oscillations. This waveform composition in urban canyons was already observed and discussed in Dragna *et al.* (2022).

For the N-wave, the shape of the waveform with the largest amplitude depends on the type of urban geometry. A sketch is shown in Fig. 7 to help with the discussion. For compact urban geometries (LCZ 1, 2, 3, 4, and 7), the waveform with the largest amplitude is obtained either at the left or at the right bottom corner of the canyon. There are two main contributions. The first arrival at $\tau = 0$ is related to the diffraction of the incident boom at the top corners of the canyon; therefore, this first arrival appears rounded. It is followed by a second arrival, due to the reflection of the incident boom on the facades of the adjacent buildings. This second arrival presents two shocks, associated with the superposition of the reflected N-wave on the diffracted arrival. For LCZ 1 that has the largest aspect ratio, the waveform with the largest amplitude is at the right bottom corner of the canyon. The first arrival originates from the combination of the two diffracted waves at the top corners. The second arrival is due to the double reflection of the incident boom first on the facade of the right-hand side building and then on that of the left-hand side building. For LCZ 2, 3, 4, and 7, that have a smaller aspect ratio than LCZ 1, the waveform with the largest amplitude is at the left bottom corner of the canyon. The first arrival is due to the boom diffracted at the top left corner of the canyon and the second arrival to the single reflection of the boom on the facade of the right-hand side building. The waveform for LCZ 7 is slightly different from the other ones. The first arrival with a rounded front shock is only separated from the second arrival by a few milliseconds, due to the small path difference, and is hardly visible. In addition, oscillations are discernible on the second arrival, due to waves diffracted by the numerous buildings of small size.

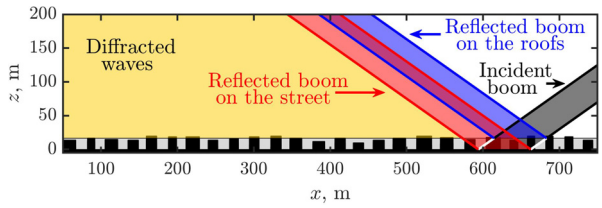

FIG. 5. (Color online) Reflection pattern of sonic boom above an urban area.

For open urban geometries (LCZ 5, 6, 8, 9, and 10), the waveform with the largest amplitude is obtained at the right bottom corner of the canyon. Only a single arrival is observed and is related to the diffraction of the incident boom at the corner. The maximum amplitude is identical for open geometries, close to 96 Pa, corresponding to the incident peak pressure increased by a factor of four. It is always higher than 96 Pa for compact geometries and reaches a maximum of 118 Pa for LCZ 2.

With the C25D wave, except for LCZ 1 for which two arrivals can be distinguished, the waveforms are composed for the other nine LCZ of a single arrival. In addition, there is no spike on the waveforms contrary to the N-wave. These two phenomena are due to the lower frequency content of the low-boom wave with respect to the N-wave. There is no clear increase in peak pressure for compact geometries either, compared to open geometries. In addition, the peak pressure for open geometries is increased but by a factor of less than four. Unlike with the N-wave, the geometrical explanation is not valid for the C25D wave. This is likely due to frequency-dependent diffraction: one can expect a purely geometrical analysis to be more applicable to a boom wave with sharp shock than to a low-boom wave. The variability of the C25D wave is mainly observed on the negative phase of the time signal.

Concerning the low frequency oscillations, a large variability can be noted in terms of frequency and amplitude for both boom waves. In the examples of waveforms for the N-wave, the oscillations are thus of significant amplitude for LCZ 3 but almost absent for LCZ 6 and their period is about 0.4 s for LCZ 1 but of 0.05 s for LCZ 7. It is shown in Secs. IV A 3 and IV B 3 that the amplitude and frequency of the post-boom oscillations vary significantly from an urban canyon to another within the same LCZ geometry.

We remind the reader that 2D urban geometries are considered. This assumes that the buildings have infinite length in the direction perpendicular to the plane of interest. For buildings of finite width, diffraction at the lateral edges of the buildings would also occur, leading to additional contributions in the canyon. Furthermore, we can also expect the frequency and amplitude of the post-boom oscillations to be different for an interrupted street canyon and to depend on the ratio of street to building lengths.

IV. ANALYSIS OF LCZ 2 AND LCZ 5

This section details the results obtained for two of the ten LCZ, representative of the two types of urban geometries, compact and open. LCZ 2 and 5 have been chosen. LCZ 2 corresponds to a city core densely built with midrise buildings and LCZ 5 to a residential area in the urban

https://doi.org/10.1121/10.0016442

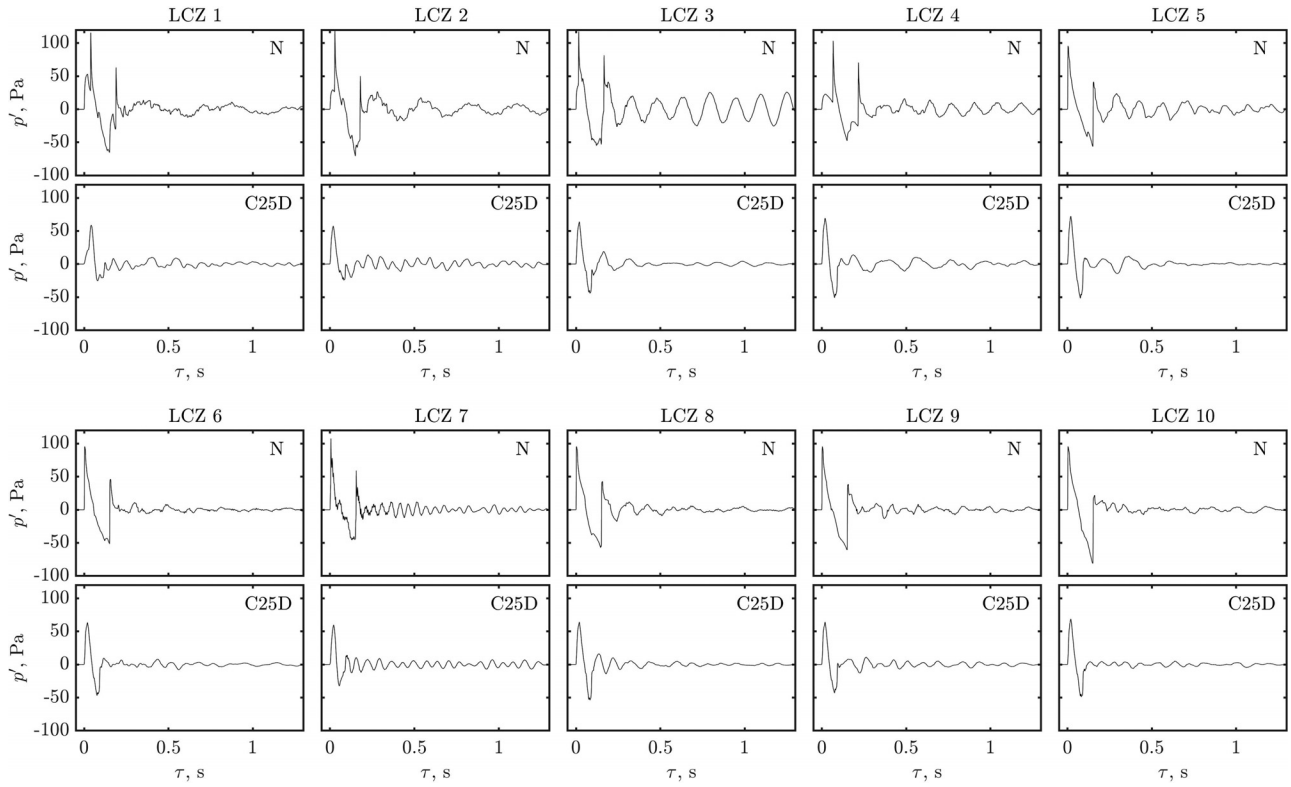

FIG. 6. Waveforms in the urban canyon having the maximum peak pressure for the ten LCZ.

periphery. The buildings in both LCZ have similar size (see Table II) and the LCZ mainly differ in aspect ratio.

A. LCZ 2—Compact midrise

Mm. 1. Video showing sonic boom propagation over the urban geometry LCZ 2 for (top) the N-wave and (bottom) the C25D wave.

The configuration LCZ 2, corresponding to a compact geometry, is studied first. The evolution of the acoustic field as the incident boom propagates over the urban profile LCZ 2 is available for the N-wave and for the C25D wave in Mm. 1.

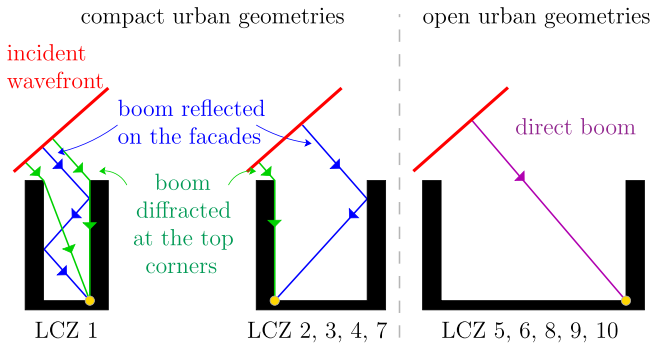

FIG. 7. (Color online) Sketch showing the contributions yielding the largest peak pressure in street canyons for compact and open urban geometries.

1. Example of waveforms

Waveforms in three street canyons for LCZ 2 are shown in Fig. 8. The canyons have been chosen as the corresponding waveforms are representative of the variability within a compact urban geometry.

In canyon A, the largest peak pressure over the urban form is observed for the N-wave with a value of 118 Pa; it is obtained at the left bottom corner of the canyon. This can be compared to the value of the peak pressure expected without buildings, equal to 48 Pa. In the middle of the canyon and at the right bottom corner, the peak pressure is largely reduced, with a value around 60–70 Pa. At the opposite, the corresponding results for the C25D show little variability: the peak pressure remains around 50 Pa at the three locations. In canyon B, the largest peak pressure is only of 80 Pa for the N-wave, compared to the value of 118 Pa in canyon A. In addition, it is obtained at the right bottom corner of the canyon, instead of the left one. Note also that the frequency of the oscillations at the tail ($\tau > 0.2$ s) is higher than in canyon A. In canyon C, the smallest peak pressure over the urban form is obtained for the N-wave, with a value of 50 Pa. This is less than half the peak pressure in canyon A. Also, observe that the peak pressure is almost the same at the three locations in that street canyon. The oscillations at the tail of the waveforms have the largest amplitude, compared to canyons A and B. Their amplitude decreases slowly with time: it is thus about 15 Pa for $\tau = 1$ s. Finally, the variability of the waveforms in canyon B and C is similar for the C25D wave and the N-wave, contrary to canyon A.

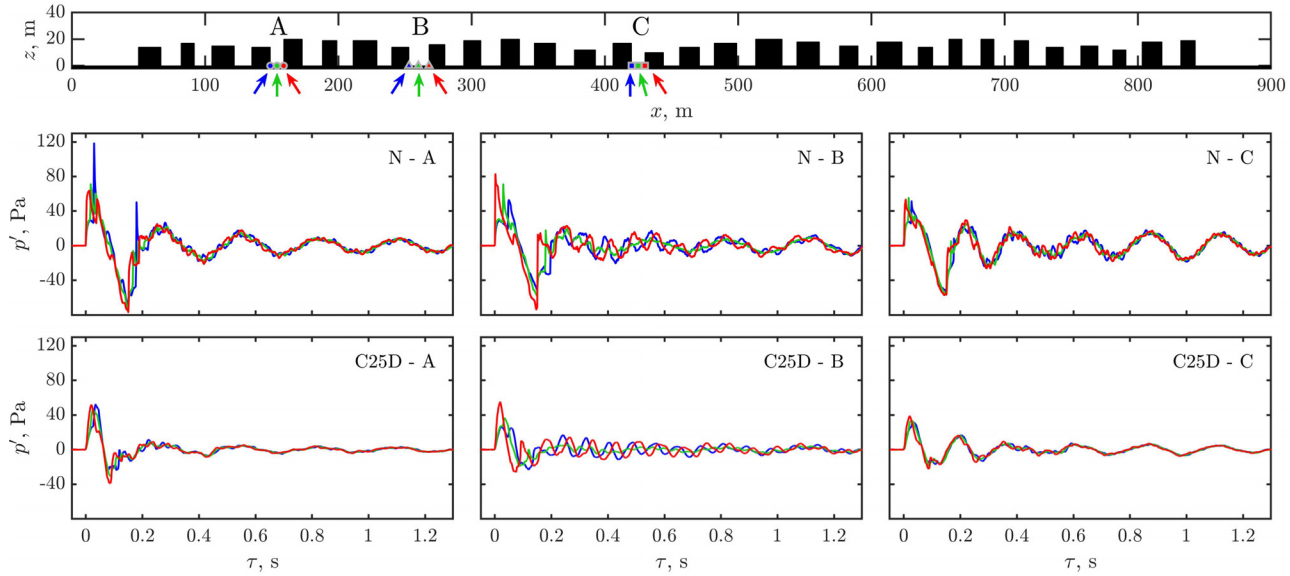

FIG. 8. (Color online) LCZ 2—Waveforms at three locations in three street canyons denoted by A, B, and C for (top) the N-wave and (bottom) C25D wave.

2. Peak pressure

To characterize the variations of the peak pressure along the urban profiles, the intensification factor (IF) is introduced. It is defined as $\mathrm{IF} = p_{\max}/p_{\mathrm{ind}}$, where $p_{\max}$ and p_{ind} are the peak values of the local waveform and of the incident waveform, respectively. The intensification factor is thus equal to one in free field, to two on a flat perfectly reflecting ground surface and to four at a 2D 90° angle corner.

The evolution of the intensification factor on the facades and roofs of the buildings and on the street is shown in canyon A for the N- and C25D waves in Fig. 9. The parameter s denotes the position along the canyon. Positions [1], [2], [3], and [4] correspond to the corners of the neighbouring buildings in the canyon. For the N-wave, the intensification factor is first equal to two above the roof of the building on the left, then sharply reduces at the top left corner of the canyon. It increases along the facade of this building and reaches a maximum of 5 at the bottom left corner. It gradually reduces along the street and the facade of the building on the right, before attaining a value of two on its facade and roof. A large decrease in the intensification factor can also be noted at the top right corner of the canyon. For the C25D wave, the evolution is significantly different. First, the intensification factor remains below two on the roofs. Next, the maximum value of IF is notably smaller, around 2.8, and is obtained at the two bottom corners of the canyon. Then, its minimum value attained on the facade of the building on the left is 0.9, which means that the peak pressure can be lower than in free-field. It should be noted that IF can also be lower than one for the N-wave; this occurs, for instance, on the facade of the building on the left in canyon C. Finally, the intensification factor for the C25D wave remains below that for the N-wave throughout the canyon.

To get a global view of the variation of IF, the intensification factor is plotted for the N- and C25D waves along the urban profiles LCZ 2 in Fig. 10, including the facades and roofs of the buildings, as well as the streets. In this figure, for x corresponding to the position of building facades, IF jumps from its minimal value to its maximal value on the facade.

As previously shown for canyon A, the intensification factor for the N-wave is equal to two on the roofs. It is usually larger than two in the streets, which implies that the urban environment leads to an increase in peak pressure compared to a flat ground. More precisely, the intensification factor is mostly between 2.5 and 3.5 for the N-wave and reaches a maximum of 5.

As observed in canyon A, the intensification factor is significantly different for the C25D wave. It is below two on the roofs. In the street of the canyons, it is consistently smaller than with the N-wave and it is regularly below two, such as in canyon C for example.

Moreover, far from the buildings ($x < 35$ m and $x > 885$ m), the intensification factor is equal to two for both boom waves and the urban environment does not influence the peak pressure. Finally, the intensification factor sharply decreases below two for both boom waves behind the last

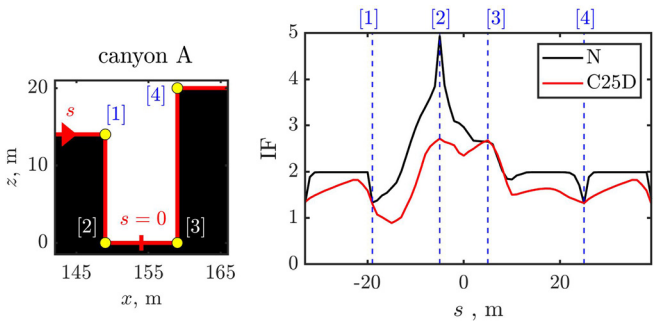

FIG. 9. (Color online) LCZ 2—Intensification factor along the street and the facade and roof of the buildings for canyon A and for both boom waves.

https://doi.org/10.1121/10.0016442

building of the profile, because of the geometrical shadow zone.

3. Low-frequency oscillations

Another noteworthy feature of the waveforms inside the street canyons is the presence of low-frequency oscillations. They have been explained by resonant modes of the street canyons in Dragna *et al.* (2022). As an example, the ESD of the acoustic pressure at the right bottom corner of canyon B is plotted in Fig. 11 for the N-wave in the low-frequency range. The corresponding ESD for flat ground is also plotted for comparison. While the variations are smooth for flat ground, the ESD in the urban canyon presents abrupt variations. In particular, two peaks centered at frequencies of 4 and 12 Hz are observed, due to the oscillations at the tail of the corresponding waveform in Fig. 8.

Figure 12 shows the ESD along the streets and building surfaces of canyons A, B, and C of the urban profile LCZ 2 for both boom waves. As a reminder, s denotes the position in the urban canyon and the positions [1], [2], [3], and [4] correspond to the corners of the neighbouring buildings in the canyon. The resonant frequencies of the first four modes determined by modelling the street canyon as an open cavity are also superimposed. They are calculated with the formula (see, for instance, Tam, 1976)

$$f_{mn} = \frac{c_0}{2}\sqrt{\left(\frac{m}{\bar{W}_\mathrm{s}}\right)^2 + \left(\frac{1+2n}{2[\bar{H}_\mathrm{b} + \alpha \bar{W}_\mathrm{s}]}\right)^2}, \tag{2}$$

where m and n are integers and α is a parameter to account for end correction effects, set to 0.2. Thus, f_{00} corresponds to the frequency of the first depth mode and f_{10} to that of the first transverse mode. Note that, for simplicity, the mean geometrical properties of the urban profiles have been considered instead of the local characteristics of each canyon.

The ESD present dark spots in the urban canyons, corresponding to the peaks illustrated in Fig. 11. These spots are centered at frequencies close to the horizontal lines showing the frequencies of the first two resonant modes f_{00} and f_{10}. Note that the modes are observed at the same frequencies for both boom waves. The mode frequency noticeably depends on the canyon considered; thus, while the depth mode is centered around a frequency close to 5 Hz for the three canyons, the first transverse mode, with an amplitude of zero at the middle of the canyon ($s = 0$), is observed at 18 Hz for canyons A and C but at 12 Hz in canyon B. The amplitude of the modes depends both on the incident boom wave and on the urban canyon considered. For instance, in canyon C, the first transverse mode has a noticeable amplitude for the N-wave in Fig. 12(a) at 18 Hz but is hardly visible for the C25D wave in Fig. 12(b). Moreover, the first transverse mode is clearly noticed in canyon B at 12 Hz with the C25D wave, contrary to canyons A and C. As a consequence, the predominant mode is not the same for all urban canyons; for the C25D wave, the first transverse mode has the largest amplitude in canyon B while the first depth mode is predominant in canyons A and C.

The centre time t_c, defined by

$$t_c = \int_0^\infty \left[p'(\tau)\right]^2 \tau \, \mathrm{d}\tau \Big/ \int_0^\infty \left[p'(\tau)\right]^2 \mathrm{d}\tau, \tag{3}$$

is introduced to characterize the lengthening of the waveforms in the urban canyons. It is the first moment of the squared acoustic pressure normalized by the signal energy. Obviously, a greater value of t_c implies a greater contribution of the late part of the waveform, mostly due to low frequency oscillations, compared to the early geometric arrivals. It also indicates a longer duration of the waveform. For instance, for the waveforms shown in Fig. 8, the centre time is equal for the N-wave to 0.19 s in canyon A, but to 0.33 s in canyon C. This can be compared to the centre time $t_{c,\mathrm{ref}}$ that would be obtained above flat ground; one finds $t_{c,\mathrm{ref}} = 0.075$ s for the N-wave which is just the half-duration of the incident N-wave boom, because of its symmetry. Therefore, the centre time is more than four times longer in canyon C than above flat ground.

The evolution of the centre time along the urban profile is plotted in Fig. 13 for both boom waves. Far from the buildings, the centre time is close to that obtained above a flat ground ($t_{c,\mathrm{ref}} = 0.075$ s for the N-wave and 0.036 s for the C25D wave). This is especially observed for $x > 850$ m; for $x < 50$ m, the leftward diffracted and reflected waves tend to increase slightly the centre time. Along the urban profile, the centre time is notably longer in the urban canyons. It shows a large variability with values from 0.14 s to 0.33 s for the N-wave, depending on the urban canyon. The variations of the centre time for the C25D wave are remarkably different to those for the N-wave: for instance, the

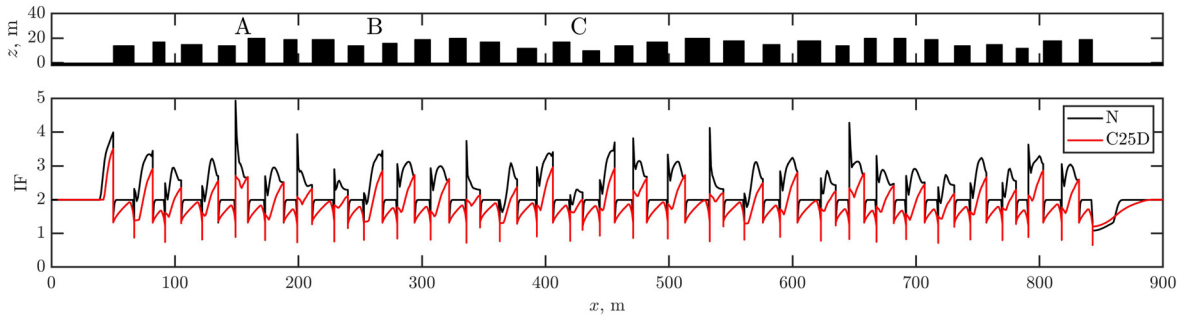

FIG. 10. (Color online) LCZ 2—Evolution of the intensification factor along the urban profile: (black) N-wave and (red) C25D wave.

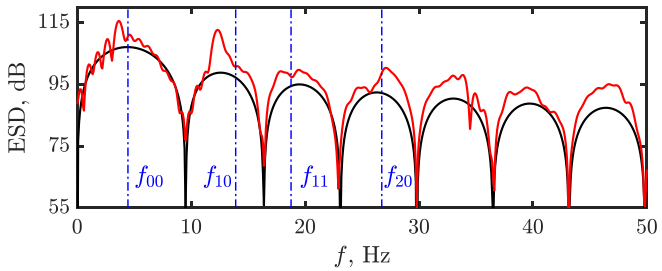

FIG. 11. (Color online) LCZ 2—Energy spectral density of the acoustic pressure for the N-wave as a function of the frequency: (red solid) at the right bottom corner of canyon B and (black solid) above a flat ground. The vertical dash-dotted lines indicate the resonant frequencies obtained from Eq. (2).

centre time in canyon C at $x = 425$ m increases much more significantly for the N-wave than for the C25D wave.

4. Noise levels

The variability of the waveforms and of its characteristics has been investigated in the previous sections. The induced variability in the perceived noise levels is now considered. The noise levels are evaluated using three metrics, that are suitable to predict human response to sonic booms (Loubeau *et al.*, 2015). The first one is Stevens' Mark VII perceived level (PL) (Stevens, 1972), which is the de facto standard metric to evaluate boom annoyance. The second one is the indoor sonic boom annoyance predictor (ISBAP), which was proposed recently (Loubeau *et al.*, 2015) in an attempt to predict indoor annoyance from the outdoor waveform. The third metric is the D-weighted sound exposure level (DSEL). This metric provides a similar variability of sound levels due to turbulence effects than PL metric for a classical N-wave; the variability is, however, reduced for low-boom waves (Leconte *et al.*, 2022). It is interesting to investigate whether this is also the case in urban environments. Hereafter, the notation PLdB and dBD is used for brevity to indicate noise levels calculated with the PL and DSEL metrics, respectively.

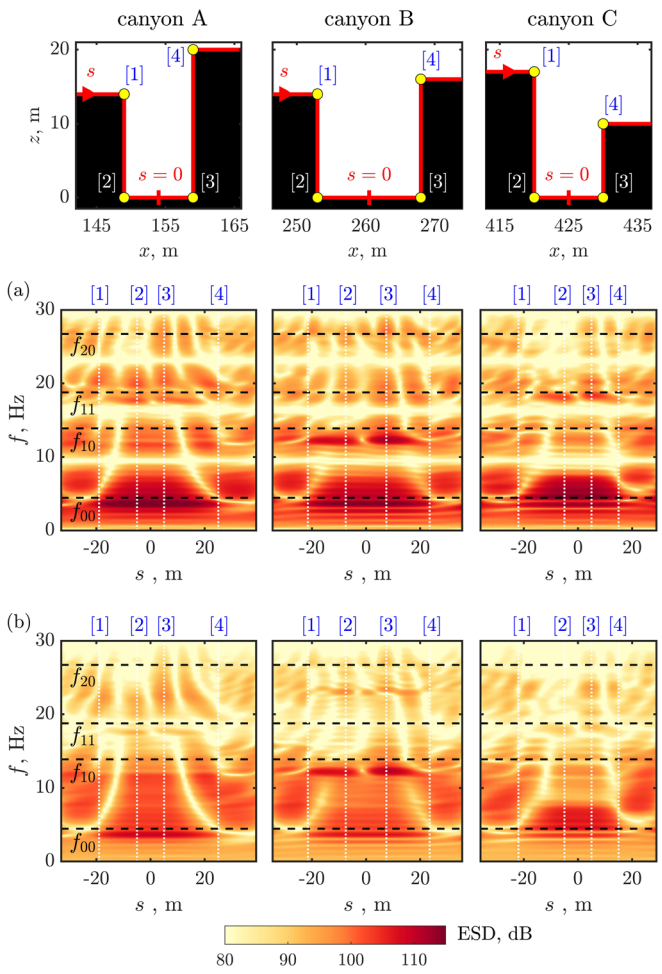

FIG. 12. (Color online) LCZ 2—Energy spectral densities as a function of the frequency along the building surfaces for the canyons A, B, and C and for (a) the N-wave and (b) the C25D wave. The horizontal dashed lines indicate the resonant frequencies obtained from Eq. (2).

Figure 14 shows the evolution of the relative perceived noise levels along the urban profile for LCZ 2 and for both boom waves. The noise levels above a flat ground are used as a reference to highlight the variations due to the urban profile. They are of 98.2 dB (PL), 105.9 dB (ISBAP), and 94.6 dB (DSEL) for the N-wave and 82.8 dB (PL), 95.3 dB (ISBAP), and 85.3 dB (DSEL) for the C25D wave. Consider first the PL metric in Fig. 14(a). In front of the first building, the relative noise levels for both boom waves increase and reach a maximum of 7 PLdB at the building corner. Behind the last building, a large decrease in the relative levels is observed with a minimum of −18.5 PLdB for the N-wave and −17.8 PLdB for the C25D wave, due to the shadow zone. These two effects were already noticed in Dragna *et al.* (2022) for an isolated building. In urban canyons, the range of variations is much smaller: the relative noise levels are between −8 and 7 PLdB for both boom waves. The local variability of the noise levels can also be appreciated. Thus, the noise levels are everywhere larger than the flat ground case in canyon A, but smaller in canyon C. In canyon B, the noise levels are reduced compared to the flat ground case in the left part of the canyon but amplified in the right part. Note also that the noise levels (relative to the flat ground case) are almost the same for both boom waves. Finally, comparing Figs. 14(a), 14(b), and 14(c), it can be remarked that the three metrics predict a similar variation of the perceived noise levels.

B. LCZ 5—Open midrise

The analysis conducted above for the compact urban geometry LCZ 2 is now performed for the open geometry LCZ 5. The evolution of the acoustic field as the incident boom wave propagates over the profile LCZ 5 is available for the N-wave and for the C25D wave in Mm. 2.

Mm. 2. Video showing sonic boom propagation over the urban geometry LCZ 5 for (top) the N-wave and (bottom) the C25D wave.

https://doi.org/10.1121/10.0016442

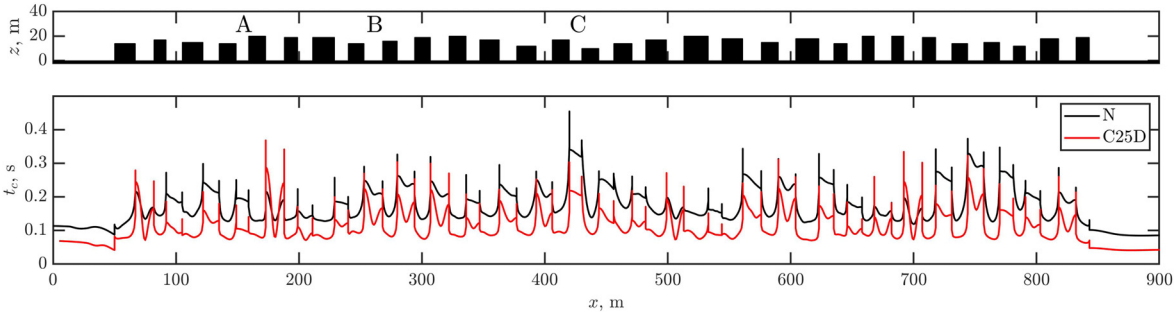

FIG. 13. (Color online) LCZ 2—Variation of the centre time along the urban profile: (black) N-wave and (red) C25D wave.

1. Example of waveforms

Examples of waveforms in three canyons of LCZ 5 are shown in Fig. 15 for the N-wave and the C25D wave. Consider first the N-wave. The waveforms in the three street canyons present a similar behavior. The maximum pressure is obtained at the right bottom corner of each canyon with a peak value between 90 and 96 Pa. At the middle and the left corner of the canyon, the first arrival, corresponding to the diffracted boom on the top left corner of the canyon, is rounded. It is followed for canyons D and E by the diffracted wave on the top right corner of the canyon (at $\tau = 0.06$ s at the middle of the canyon and $\tau = 0.12$ s at its left corner), with a much smaller amplitude. For canyon F, the second arrival in the middle of the canyon is the reflected wave on the facade of the right-hand side building and has a larger amplitude, around 60 Pa. This difference with the waveforms in canyons D and E is due to the smaller width of canyon F. In addition, low-frequency oscillations are still noticed on the waveforms for $\tau > 0.2$ s. They exhibit also a large variability in terms of amplitude, decay rate, and frequency. Thus, oscillations have a larger amplitude and period in canyon E than in F. Moreover, the oscillations rapidly decay with time in D compared to E, which may be due to the height of the buildings, smaller in canyon D than in E. These conclusions are still relevant for the C25D wave. In particular, the maximum value of peak pressure is also obtained at the right bottom corner of each canyon and the decay rate, frequency, and amplitude of the post-boom oscillations show a comparable variability between the three canyons.

2. Peak pressure

The intensification factor is shown along the urban profile for the open geometry LCZ 5 in Fig. 16, using the same representation than in Fig. 10. Compared to the compact geometry LCZ 2 in Fig. 10, the variation of the intensification factor is completely different. A similar pattern is observed along each building of the profile. IF first increases in front of each building and reaches a maximum at the bottom corner of the building, with a value close to four for the

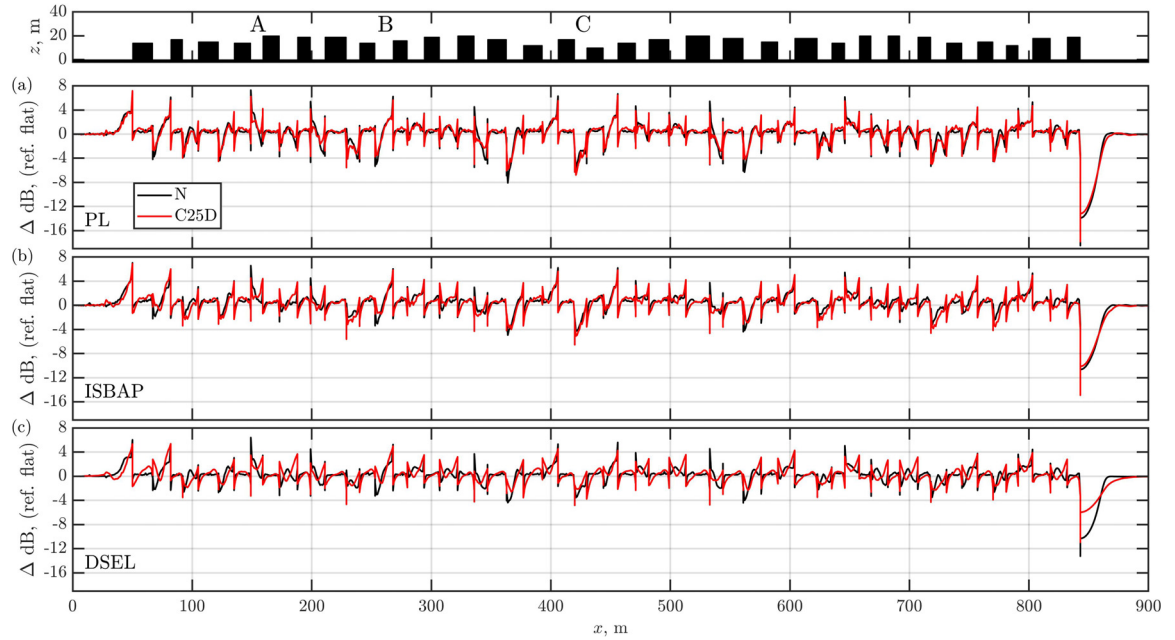

FIG. 14. (Color online) LCZ 2—Evolution of the perceived noise levels along the urban profile using metrics (a) PL, (b) ISBAP, and (c) DSEL for (black) the N-wave and (red) C25D wave.

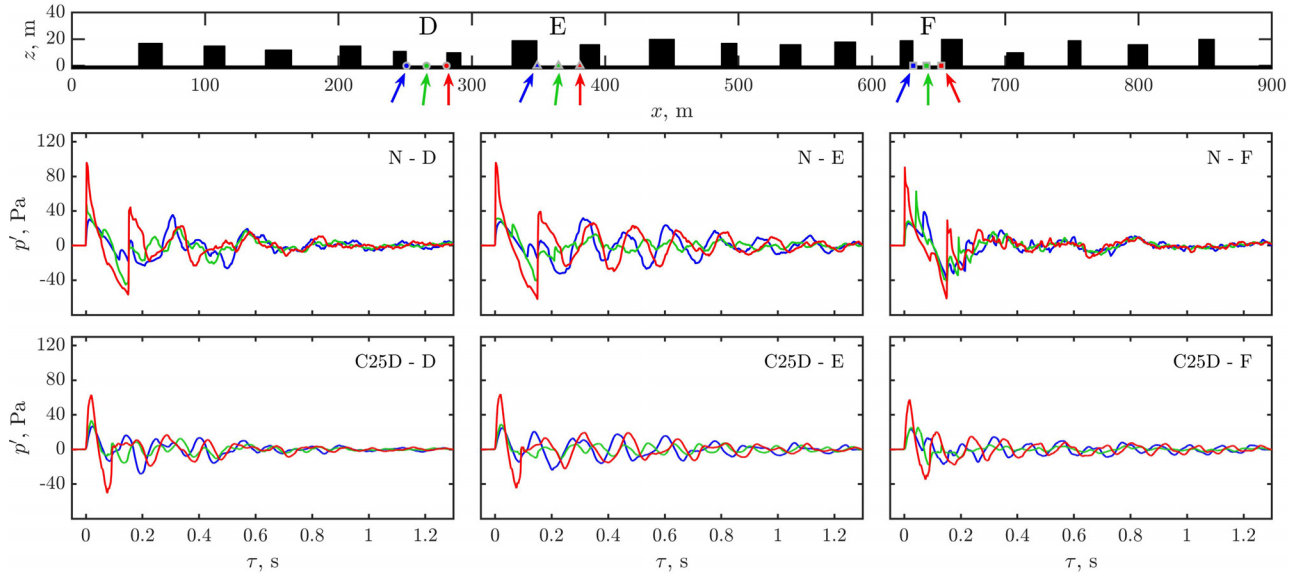

FIG. 15. (Color online) LCZ 5—Waveforms at three locations in three street canyons denoted by D, E, and F for (top) the N-wave and (bottom) the C25D wave.

N-wave and slightly lower for the C25D wave. It decreases along the front facade. On the roof, IF is equal to two for the N-wave; for the C25D wave, it increases along the roof and approaches two for sufficiently wide buildings. Finally, IF decreases below two along the rear facade of the building, before increasing again along the street, moving away from the building. This behavior corresponds to the case of an isolated building, as discussed in Dragna *et al.* (2022).

3. Low-frequency oscillations

The ESD along the streets and building surfaces of canyons D, E, and F are shown in Fig. 17 for both boom waves. As for LCZ 2, the horizontal lines indicate the frequency of the first three resonant modes of the canyon using Eq. (2). The dark spots indicate the presence of modes. Their frequency, especially for canyons D and E, is closely predicted by Eq. (2). As for LCZ 2, the frequency and amplitude of the modes significantly depend on the urban canyon considered. In addition, the frequency of the first depth mode f_{00} is close for LCZ 2 and 5. Indeed, it depends mostly on the mean building height, which is the same for both LCZs. The main difference is for transverse modes, which appear at lower frequencies due to the larger street width.

Figure 18 shows the evolution of the centre time along the urban profile for LCZ 5 and for the N-wave and C25D wave. The centre time is much longer in the left part of the canyons. Thus, the centre time for the N-wave reaches for most canyons in LCZ 5 a value higher than 0.3 s in the left part but rarely exceeds 0.15 s in the right part. This is different from LCZ 2 in Fig. 13 for which the centre time is more homogeneous in the urban canyons. This can be explained by two reasons. First, for open geometries, the left part of the canyon is in the shadow zone of the left-hand side building, which induces a reduction of the early energy ($\tau < 0.2$ s). Second, the contribution due to the diffraction of the incident boom and reflected boom on the ground at the facade of the right-hand side building arrives later on the left part of the canyon, because of the larger canyon width. It has a significant amplitude, that leads to an increase in the late energy ($\tau > 0.2$ s).

4. Noise levels

The noise levels relative to the flat ground case are plotted along the urban profile LCZ 5 in Fig. 19 for the N-wave and the C25D wave, using the three metrics. As for the

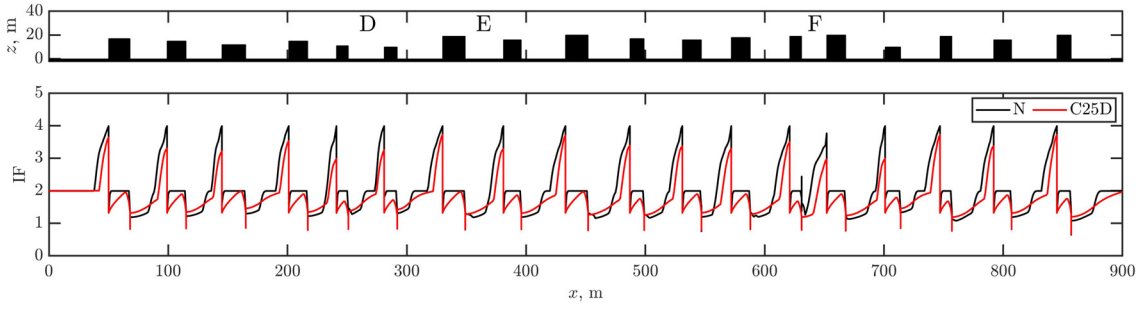

FIG. 16. (Color online) LCZ 5—Evolution of the intensification factor along the urban profile: (black) N-wave and (red) C25D wave.

https://doi.org/10.1121/10.0016442

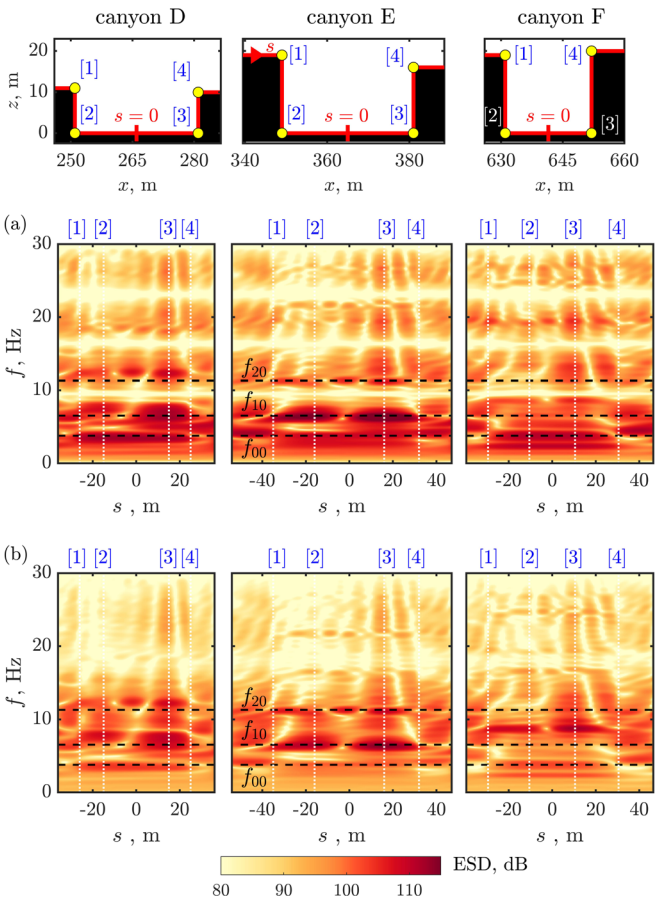

FIG. 17. (Color online) LCZ 5—Energy spectral densities as a function of the frequency along the building surfaces for the canyons D, E, and F for (a) the N-wave and (b) the C25D wave. The horizontal dashed lines indicate the resonant frequencies computed from Eq. (2).

intensification factor, a similar pattern is observed around each building. For the PL and ISBAP metrics in Figs. 19(a) and 19(b), respectively, the evolution of the noise levels is identical for the N-wave and the low-boom wave: the noise levels increase by a maximum of 7 dB in front of the building, are equal to those for the flat ground case above the roof, decrease sharply in the shadow zone behind the building and then continuously increase to recover their values without building sufficiently far from it. The minimum value of the relative noise levels depends on the canyon: for the N-wave, it is between –13 and −12 PLdB for most canyons but is equal to −7.5 PLdB for canyon F. The corresponding values for the C25D wave are 1 to 2 PLdB higher. In addition, the minimum value of the relative noise levels with the ISBAP metric is consistently higher than with the PL metric by 1–2 dB. Overall, the range of variations of the relative noise levels in the street canyons is significantly wider than for LCZ 2, for which it was limited to −8 to 7 dB (see Fig. 14). Finally, the evolution of the noise levels with the DSEL metric in Fig. 19(c) is notably different for the N-wave and the low-boom wave. For the N-wave, it is comparable to that observed with the PL and ISBAP metrics. For the C25D wave, however, the relative noise levels are significantly higher in the shadow zone behind the buildings, leading to a reduced variability of the relative noise levels, between –4 and 6 dBD.

C. Discussion

The aspect ratio, defined from mean properties of the urban geometry, is a global indicator of the geometry compactness. For open geometries such as LCZ 5, the variability between canyons was shown to be small in terms of intensification factor and noise levels. On the contrary, it is significant for compact geometries, as exemplified for LCZ 2.

For compact geometries, the main parameter governing the local variations of the intensification factor and the noise levels between urban canyons is the difference in height of the neighbouring buildings. Typically, if the building on the left is smaller than the one on the right, the intensification factor and the noise levels are usually large in the canyon. On the other hand, if the building on the left is higher than the one on the right, these two parameters tend to reduce. This can be observed by comparing the intensification factor and the noise levels for canyons A and C in Figs. 10 and 14.

In order to explain qualitatively this behavior, a geometrical analysis is conducted. Figure 20 shows the propagation of rays originating from an incident wavefront towards an urban canyon for five configurations of buildings. Thereafter, the parameter $\Delta H_b = H_{b,r} - H_{b,l}$ denotes the building height difference, where $H_{b,l}$ and $H_{b,r}$ are respectively the height of buildings on the left and on the right. Figure 20(a) is the reference case with two buildings of the same height, i.e., $\Delta H_b = 0$. The red thick line represents the part of the incident wavefront reaching the canyon. Its length indicates the amount of acoustic energy entering the canyon. For Fig. 20(b), the building on the right is higher than the one on the left

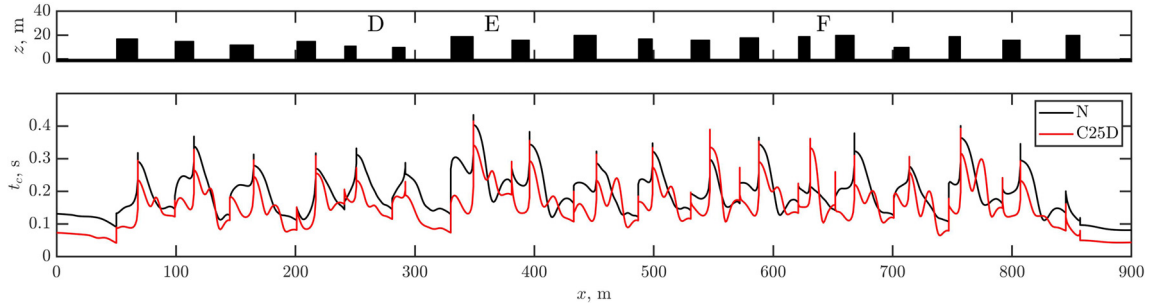

FIG. 18. (Color online) LCZ 5—Variation of the centre time along the urban profile: (black) N-wave and (red) C25D wave.

($\Delta H_b > 0$): the rays impacting the facade of the right-hand side building are reflected towards the canyon. This induces a larger amount of acoustic energy entering the canyon, compared to Fig. 20(a). This effect is amplified when the right-hand side building is higher, up to a difference in building height equal to $\Delta H_b = W_s/\tan\theta = \sqrt{M^2-1}\,W_s$. For higher buildings, as illustrated in Fig. 20(c), no further increase in the energy entering the canyon is expected. For Fig. 20(d), the building on the left is higher than the one on the right ($\Delta H_b < 0$) and shields the canyon from a significant part of the incident wavefront. Figure 20(e) is the limiting case for which no acoustic rays enter the canyon. From geometric considerations, this happens when $\Delta H_b \leq -W_s/\tan\theta = -\sqrt{M^2-1}\,W_s$. For such values of ΔH_b, the canyon lies entirely in the shadow zone created by the left-hand side building.

For $M = 1.6$, one has $\sqrt{M^2-1} = 1.25$. Therefore, the canyon lies entirely in the shadow zone for $\Delta H_b/W_s \leq -1.25$ and a maximum amplification is expected in the canyon for $\Delta H_b/W_s \geq 1.25$. For LCZ 2, $\Delta H_b/W_s$ is between –0.7 and 0.6. The minimum value is obtained in canyon C and the maximum value in canyon A, which is in agreement with the remarks made earlier on the intensification factor and noise levels.

This analysis is purely energetic and provides a rough indication of the evolution of the intensification factor and noise levels in an urban geometry. Furthermore, it is relevant only for compact geometries such as LCZ 2, and not for open geometries like LCZ 5. Indeed, the difference in the height of the neighbouring buildings does not play a role in the geometrical field when the buildings are sufficiently far from each other and can be considered as isolated, which is the case for open geometries.

V. STATISTICAL ANALYSIS

This section presents a comparative analysis of the noise levels for the ten LCZ. Note that the statistics are computed from the results of the 900 m long profile. They may differ from those determined for a profile of infinite length with the same statistical characteristics (building height and width and street width).

Figure 21 shows the cumulative probability of the noise levels inside the urban canyons for the ten LCZ, i.e., along the facades of the buildings and along the streets (the noise levels on the roof are discarded). As done before, the noise levels relative to their value for the flat ground case are considered, using the three metrics PL, ISBAP, and DSEL. Let us examine first the distributions for the N-wave plotted in solid lines. The cumulative probability distribution has a different behavior for compact and open geometries. For compact geometries (LCZ 1–4 and 7), the relative noise levels are distributed continuously, whereas open geometries (LCZ 5, 6, and 8–10) present a staircase evolution, with increments for relative noise levels of 0 and 4 dB. Indeed, these values are often obtained for open geometries: 0 dB in the middle of canyons, sufficiently far from the buildings, and 4 dB in the illuminated zone in front of isolated buildings (Dragna *et al.*, 2022). The variability within open or compact geometries is also noticeable. For instance, for open geometries, the increment at 0 dB is large for LCZ 8–10. This is due to the small aspect ratio for these LCZ (around 0.2): the canyons are large, implying that the influence of buildings is negligible in most of the urban canyon. On the contrary, the increment at 0 dB is hardly visible for LCZ 5, because of the larger aspect ratio. The distributions for the N-wave slightly depend on the metric used for the noise

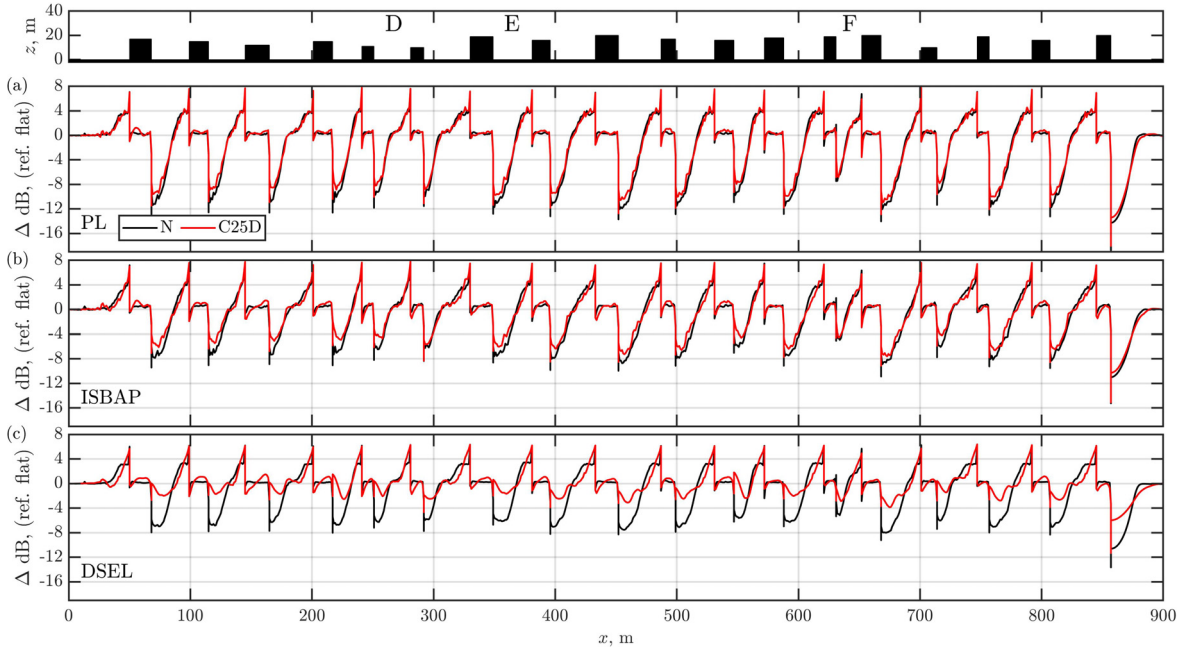

FIG. 19. (Color online) LCZ 5—Evolution of the perceived noise levels along the urban profile using the metrics (a) PL, (b) ISBAP, and (c) DSEL for (black) the N-wave and (red) C25D wave.

https://doi.org/10.1121/10.0016442

levels. In particular, the PL metric predicts a larger reduction of the noise levels than ISBAP and DSEL in shadow zones (see, e.g., LCZ 5 for relative noise levels below –3 dB).

The cumulative probability distributions of relative noise levels are shown in Fig. 21 for the C25D wave in dashed lines. They are very close to those for the N-wave for the PL and ISBAP metrics. Concerning the DSEL metric, the distributions are comparable for compact urban profiles (LCZ 1–4 and 7), although they are shifted towards higher values of relative noise levels for LCZ 3 and 7, compared to those for the N-wave. For open urban profiles (LCZ 5, 6, and 8–10), the distributions are significantly different from those for the N-wave: in particular, the occurrence of relative noise levels below –3 dBD is largely reduced. This behavior was noticed in Fig. 19(c) for LCZ 5.

To compare the results for the ten LCZ, the statistics of the noise levels relative to the flat ground case are shown as boxplots in Fig. 22. First, consider the levels for the N-wave, using the PL metric in Fig. 22(a). The red horizontal line inside the box indicates the median of the relative noise levels. For most LCZ, it is close to 0 PLdB (within ±0.5 PLdB). The largest deviations are obtained for LCZ 1 with a median of −1 PLdB, and for LCZ 7 with a median of 0.6 PLdB. This indicates that, while local variations are significant, there is on average no large increase or reduction of noise levels compared to the flat ground case due to urban environments, regardless of the geometry. The length of the box in Fig. 22 corresponds to the interquartile range (IQR), which is the difference between the third and first quartile. For information, quartiles divide the data set into four parts: the first quartile is the 25th percentile, the second quartile is the 50th percentile, corresponding to the median, and the third quartile is the 75th percentile. IQR indicates the spread of the data. It is smaller for compact geometries than for open geometries. In particular, compare IQR for LCZ 2 and 5, which have buildings of the same dimensions but differ in the aspect ratio: IQR is equal to 3.1 PLdB for LCZ 2 and 12.8 PLdB for LCZ 5. Again, noise levels tend to be more uniform in a compact geometry than in an open geometry. Finally, the minimum and maximum values of the relative noise levels are given by the boundaries of the whiskers in Fig. 22. The maximum value is very close for the ten LCZ, between 7.2 and 8.0 PLdB. The minimum value is however significantly different. It is large for open geometries, between –14.0 and –11.8 PLdB. For compact geometries, it is on average higher with a value between −12.2 and –5.9 PLdB. The boxplots for the N-wave with the ISBAP and DSEL metrics in Figs. 22(b) and 22(c) show a close similarity to those with the PL metric in Fig. 22(a). The minimum value of the relative noise levels is, however, greater than with PL. Furthermore, IQR is reduced for open geometries (LCZ 5, 6, 8–10) with ISBAP and even more with DSEL. For instance, for LCZ 5, the minimum value of the relative noise levels is –14.0 dB (PL), –10.9 dB (ISBAP), and –9.2 dB (DSEL), and IQR is 12.8 dB (PL), 9.7 dB (ISBAP), and 9.2 dB (DSEL).

Let us now consider the boxplots for the low-boom wave. For PL in Fig. 22(d), the boxplots are similar to those for the N-wave in Fig. 22(a). In particular, the median is within ±0.5 PLdB for most LCZ, but reduced to −1 PLdB for LCZ 1 and to –0.8 for LCZ 5 and increased to 1.1 PLdB for LCZ 7. IQR is similar for compact geometries but slightly reduced for open geometries. As an example, it is equal for LCZ 5 to 11.4 PLdB, compared to 12.8 PLdB for the N-wave. Concerning ISBAP in Fig. 22(e), the conclusions drawn from the comparison of the boxplots for PL and ISBAP for the N-wave also apply for the C25D wave. However, one can notice a marked increase in the median for LCZ 7 to 2.4 dB (ISBAP). Finally, the metric DSEL in Fig. 22(f) presents significantly different behavior for the two boom waves. The boxplots show a reduced variability of the noise levels using this metric for the C25D wave in regards to urban environment, compared to the N-wave. In particular, note the reduction of IQR for open geometries. Thus, the maximum of IQR, obtained for LCZ 5, is equal to 3.7 dBD for the C25D wave and 9.2 dBD for the N-wave. As a consequence, IQR is almost the same for all LCZ classes. In addition, the minimum value of the relative noise levels is equal to −7 dBD (obtained for LCZ 1 and 10), compared to −9.1 dBD (for LCZ 1) for the N-wave. As a conclusion, it is found that the noise level variability in an urban environment significantly depends on the choice of the boom metric for the low-boom wave, contrary to the N-wave: PL and ISBAP show a similar variability for the N-wave and the low boom wave, but DSEL provides a reduced variability for the low-boom wave. This echoes corresponding findings reported by Leconte *et al.* (2022) for the case of sonic boom propagation in a turbulent atmosphere.

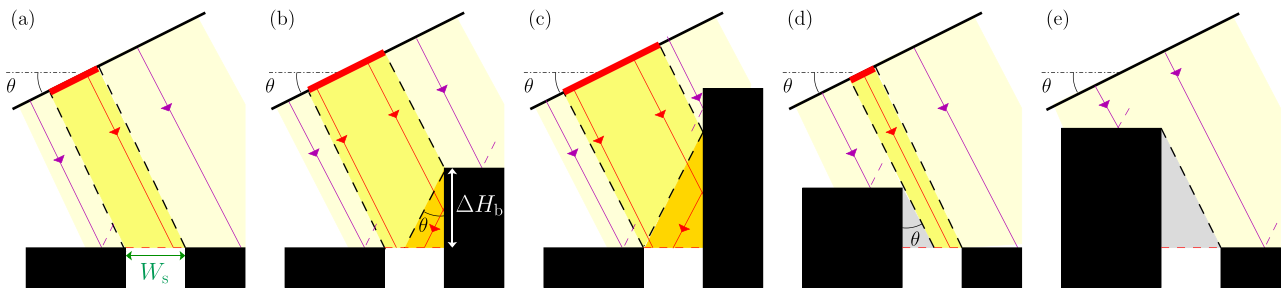

FIG. 20. (Color online) Sketch showing the rays originating from an incident wavefront interacting with the neighbouring buildings of an urban canyon with different heights for five configurations. See text for details.

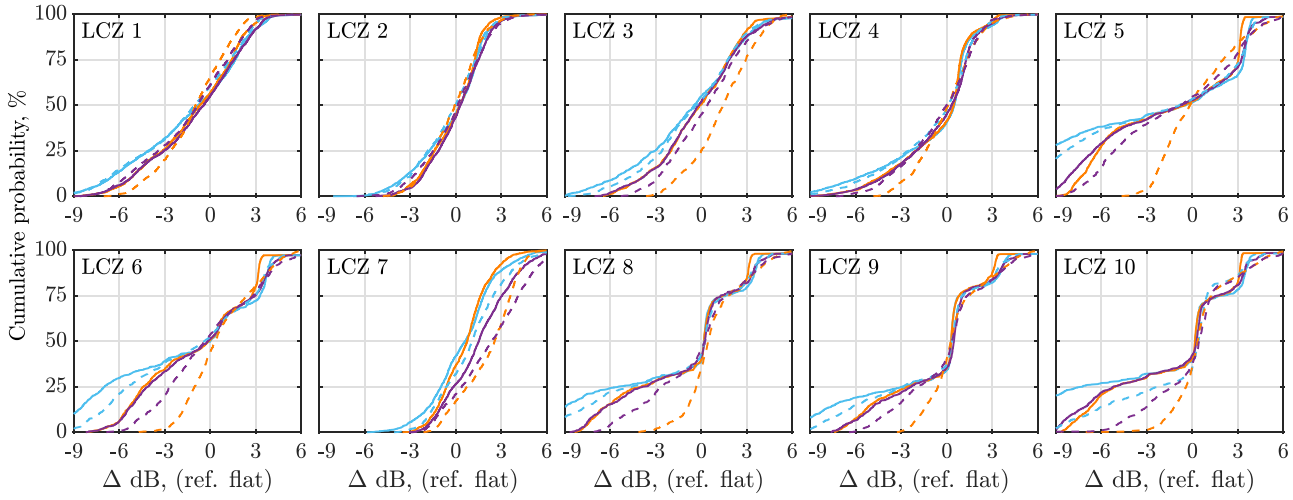

FIG. 21. (Color online) Cumulative probability of the perceived noise levels inside the urban canyons, using the metrics (light blue) PL, (violet) ISBAP, and (orange) DSEL for the ten LCZ. Results are shown for the N-wave in solid lines and the C25D wave in dashed lines.

VI. CONCLUSIONS

Sonic boom propagation over urban areas has been investigated for two boom waves, a classical N-wave and a low-boom wave. Ten geometries, generated from the LCZ classification, have been considered as representative of urban environments. Two behaviors have been distinguished, depending on the aspect ratio of urban canyons. Compact geometries, characterized by a large aspect ratio, show a significant variability between the canyons in terms of peak pressure, especially for the N-wave, and noise levels. The main parameter governing local variations is the difference in the height of the buildings. Open geometries, with a small aspect ratio, present low variability: the evolution of the intensification factor and the noise levels along each building shows a similar pattern, corresponding to one of the isolated buildings. For both boom waves, the maximum increase in the noise levels is similar for the ten geometries, between 7 and 8 dB. Conversely, the largest reduction is highly dependent on the urban geometry considered. A statistical analysis of the noise levels has been performed. The distributions of noise levels in urban canyons are less spread for compact geometries than for open ones. The variability of the noise levels slightly depends on the choice of the boom metric for the N-wave. For the low-boom wave, the variability is comparable to that of the N-wave using PL or ISBAP metrics. It is, however, reduced using the DSEL metric for open urban geometries. Overall, the median of the noise levels relative to the flat ground case is close to zero for both boom waves and for the three metrics, implying that there are as many locations within the street

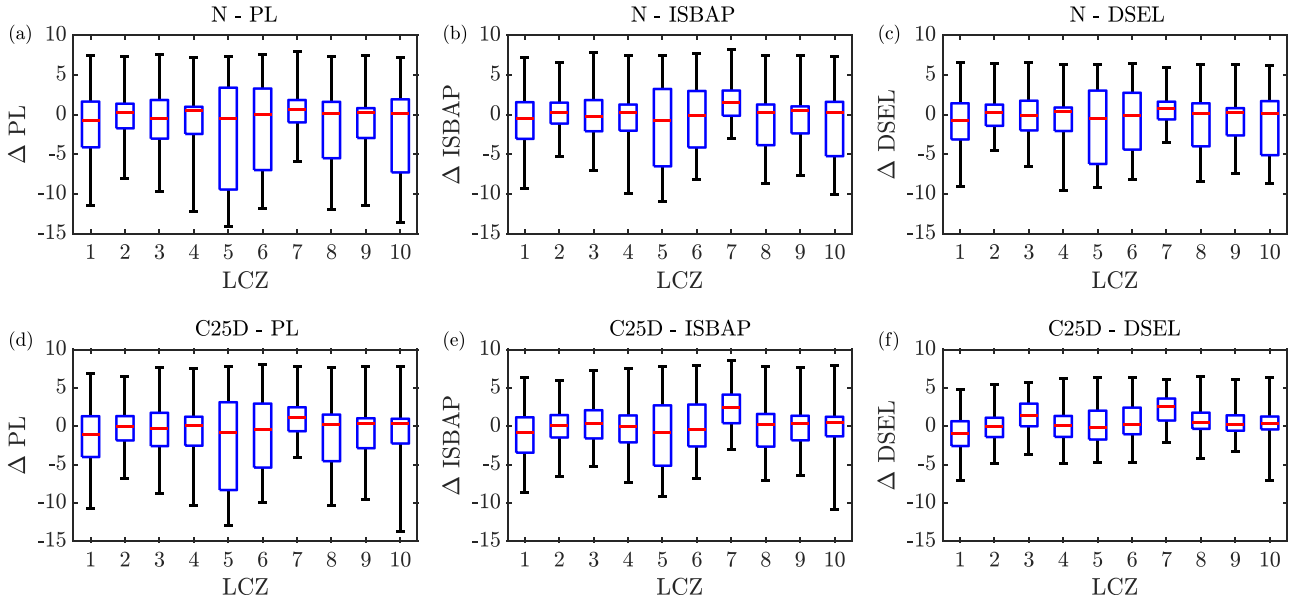

FIG. 22. (Color online) Boxplots of the noise levels relative to the flat ground case for (top) the N-wave and (bottom) C25D wave, using the metrics (left) PL, (middle) ISBAP and (right) DSEL.

canyons where noise levels increase or decrease, compared to flat ground. Finally, low-frequency oscillations have been noticed at the tail of waveforms in the urban canyons for both open and compact geometries. They also present a large variability between canyons in terms of frequency, amplitude, and decay rate.

There are several potential extensions to this work. First, as 2D simulations have been performed, it would be worthwhile investigating three-dimensional effects on reflection and diffraction by the buildings. In addition, the study has been restricted to an homogeneous atmosphere at rest. It will be interesting to study meteorological effects on sonic boom propagation over urban areas, as done by Hornikx *et al*. (2018) for application to road traffic noise. Furthermore, land covers are also defined for each of the LCZ class. Ground effect can thus also been considered in future work. Finally, the buildings had a simple rectangular shape and their facades were perfectly reflecting. Diffusive reflection due to surface irregularities can however have a large impact on sound fields inside urban canyons (Van Renterghem *et al*., 2006). A more detailed description of the building geometry could be considered as well.

ACKNOWLEDGMENTS

This project has received funding from the European Union's Horizon 2020 research and innovation programme under Grant No. 769896 (RUMBLE). This publication reflects only the author's view and the Innovation and Networks Executive Agency (INEA) is not responsible for any use that may be made of the information it contains. It was performed within the framework of the LABEX CeLyA (ANR-10-LABX-0060) of Université de Lyon, within the program "Investissements d'Avenir" (ANR-16-IDEX-0005) operated by the French National Research Agency (ANR). This work was granted access to the HPC resources of PMCS2I (Pôle de Modélisation et de Calcul en Sciences de l'Ingénieur et de l'Information) of Ecole Centrale de Lyon and PSMN (Pôle Scientifique de Modélisation Numérique) of ENS de Lyon, members of FLMSN (Fédération Lyonnaise de Modélisation et Sciences Numériques), partner of EQUIPEX EQUIP@MESO and IDRIS (Institut du Développement et des Ressources en Informatique Scientifique) under the allocation 2021–02203 made by GENCI (Grand Equipement National de Calcul Intensif).

Bauer, A. B., and Bagley, C. J. (**1970**). "Sonic boom modeling—Investigation of topographical and atmospheric effects," Report No. FAA-NO-70-10 1-212 (Douglas Aircraft Co, Long Beach, CA).

Bogey, C., and Bailly, C. (**2004**). "A family of low dispersive and low dissipative explicit schemes for flow and noise computations," J. Comput. Phys. **194**, 194–214.

Brooks, J. D., Beasley, W. D., and Barger, R. L. (**1970**). "Laboratory investigation of diffraction and reflection of sonic booms by buildings," Report No. NASA TN D-5830 1-22 (NASA, Washington, DC).

Ching, J., Mills, G., Bechtel, B., See, L., Feddema, J., Wang, X., Ren, C., Brousse, O., Martilli, A., Neophytou, M., Mouzourides, P., Stewart, I., Hanna, A., Ng, E., Foley, M., Alexander, P., Aliaga, D., Niyogi, D., Shreevastava, A., Bhalachandran, P., Masson, V., Hidalgo, J., Fung, J., Andrade, M., Baklanov, A., Dai, W., Milcinski, G., Demuzere, M., Brunsell, N., Pesaresi, M., Miao, S., Mu, Q., Chen, F., and Theeuwes, N. (**2018**). "WUDAPT: An urban weather, climate, and environmental modeling infrastructure for the Anthropocene," Bull. Am. Meteorol. Soc. **99**(9), 1907–1924.

Cho, S.-L. T., and Sparrow, V. W. (**2011**). "Diffraction of sonic booms around buildings resulting in the building spiking effect," J. Acoust. Soc. Am. **129**(3), 1250–1260.

Demuzere, M., Kittner, J., Martilli, A., Mills, G., Moede, C., Stewart, I. D., van Vliet, J., and Bechtel, B. (**2022**). "A global map of local climate zones to support earth system modelling and urban-scale environmental science," Earth Syst. Sci. Data **14**(8), 3835–3873.

Dragna, D., Emmanuelli, A., Ollivier, S., and Blanc-Benon, P. (**2022**). "Sonic boom reflection over an isolated building and multiple buildings," J. Acoust. Soc. Am. **151**(6), 3792–3806.

Emmanuelli, A., Dragna, D., Ollivier, S., and Blanc-Benon, P. (**2021**). "Characterization of topographic effects on sonic boom reflection by resolution of the Euler equations," J. Acoust. Soc. Am. **149**(4), 2437–2450.

Hidalgo, J., Dumas, G., Masson, V., Petit, G., Bechtel, B., Bocher, E., Foley, M., Schoetter, R., and Mills, G. (**2019**). "Comparison between local climate zones maps derived from administrative datasets and satellite observations," Urban Clim. **27**, 64–89.

Hornikx, M., Dohmen, M., Conen, K., van Hoof, T., and Blocken, B. (**2018**). "The wind effect on sound propagation over urban areas: Predictions for generic urban sections," Build. Environ. **144**, 519–531.

Leconte, R., Chassaing, J. C., Coulouvrat, F., and Marchiano, R. (**2022**). "Propagation of classical and low booms through kinematic turbulence with uncertain parameters," J. Acoust. Soc. Am. **151**(6), 4207–4227.

Loubeau, A., and Coulouvrat, F. (**2009**). "Effects of meteorological variability on sonic boom propagation from hypersonic aircraft," AIAA J. **47**(11), 2632–2641.

Loubeau, A., Naka, Y., Cook, B., Sparrow, V., and Morgenstern, J. (**2015**). "A new evaluation of noise metrics for sonic booms using existing data," AIP Conf. Proc. **1685**, 090015.

Maglieri, D., Bobbitt, P., Plotkin, K., Shepherd, K., Coen, P., and Richwine, D. (**2014**). "Sonic boom: Six decades of research," Technical Report NASA/SP-2014-622, L-20381, NF1676L-18333 (NASA, Washington, DC), pp. 1–539.

NASA (**2021**). "NASA's low-boom flight demonstration," https://www.nasa.gov/X59/ (Last viewed November 5, 2021).

Pawlowski, J., Graham, D., Boccadoro, C., Coen, P., and Maglieri, D. (**2005**). "Origins and overview of the shaped sonic boom demonstration program," in *43rd AIAA Aerospace Sciences Meeting and Exhibit*, January 10–13, Reno, NV, AIAA Paper 2005-5, pp. 1–14.

Rallabhandi, S. K., and Loubeau, A. (**2019**). "Summary of propagation cases of the second AIAA sonic boom prediction workshop," J. Aircr. **56**(3), 876–895.

Stevens, S. S. (**1972**). "Perceived level of noise by Mark VII and decibels (E)," J. Acoust. Soc. Am. **51**(2), 575–601.

Stewart, I. D., and Oke, T. R. (**2012**). "Local climate zones for urban temperature studies," Bull. Am. Meteorol. Soc. **93**(12), 1879–1900.

Tam, C. K. W. (**1976**). "The acoustic modes of a two-dimensional rectangular cavity," J. Sound Vib. **49**(3), 353–364.

Ting, L., and Pan, Y. S. (**1968**). "Report on sonic boom studies. Part II - Incidence of N-waves on structures," in *Second Conference on Sonic Boom Research*, May 9–10, Washington, DC NASA SP-180, edited by I. R. Schwartz, pp. 89–98.

Van Renterghem, T., Salomons, E., and Botteldooren, B. (**2006**). "Parameter study of sound propagation between city canyons with a coupled FDTD-PE model," Appl. Acoust. **67**, 487–510.

Yamashita, R., and Nikiforakis, N. (**2021**). "Numerical simulation of multiple reflections and diffractions of sonic boom around buildings," AIAA J. **59**(7), 2478–2489.